Quantum-state-controlled reactions between molecular radicals and ions

James Greenberg,[1] Philipp C. Schmid,[1] Mikhail Miller,[1] John F. Stanton,[2] and H. J. Lewandowski[1,*]
[1]*JILA and the Department of Physics, University of Colorado, Boulder, Colorado 80309-0440, USA*
[2]*Quantum Theory Project, Departments of Chemistry and Physics, University of Florida, Gainesville, Florida 32611, USA*

(Received 22 June 2018; published 13 September 2018)

Chemical reactions between ions and molecular radicals are important in both terrestrial and extraterrestrial environments. However, due to the challenge of creating dense, pure samples of both species, very few studies have been performed in the laboratory. We present the first measurement of a state-controlled reaction between a radical and an ion, where the Ca^+ cation and the NO radical molecule combine to form CaO^+ and a nitrogen atom. The charge transfer between Ca^+ and NO is simultaneously observed. We utilize a linear Paul ion trap coupled to a time-of-flight mass spectrometer to make direct, simultaneous measurements of multiple ionic product channels. We demonstrate control over the reaction rates by tuning of the excited-state population of the laser cooled $^{40}Ca^+$. This control, coupled with a sensitive detection technique, enables precise measurement of the rate constants and branching ratios for this reaction.

DOI: 10.1103/PhysRevA.98.032702

I. INTRODUCTION

Ions and free radicals play important roles in the chemistry of the interstellar medium [1,2], in many combustion processes [3,4], and in planetary atmospheres [5,6]. Therefore, studying reactions between these species in the laboratory is useful for developing models of the chemical dynamics in these environments. In addition to its importance to interstellar medium chemistry, radical-ion chemistry is interesting to explore, as reactions may proceed in a fundamentally different manner from stable molecule-ion reactions. For example, radical species such as OH, CH, and NH may abstract an H atom or other neutral entities from the ion. Alternatively, they might readily add to multiple bonds in the ion, acting as a classical electrophile, or insert into single bonds to form 3-centered three-electron intermediates. Perhaps most significant, reactions between radicals and ions are predicted to be barrierless [7–10]; therefore rapid and appreciable reactions can occur at the low temperatures of important astronomical environments, and these likely play a role in the foundations of the chemical complexity of the universe. Consequently, it is imperative to study these reactions in low-temperature environments, where an exquisite level of detail can be extracted about these fully quantum mechanical systems. Finally, the same level of detail that can be extracted from low-temperature experiments offers the chance to anchor advanced theoretical treatments of molecular phenomena [11–13].

Even with the considerable potential for increasing our understanding of gas-phase chemical reactions, experimental studies of ion-radical reactions are extremely rare [14–16]. This is because laboratory measurements of ion-radical reactions have been notoriously challenging to make, due to the difficulty of creating dense, pure samples of these reactants. Ion densities are limited by the Coulomb repulsion between molecules. Radicals, in most cases, must be created *in situ* by breaking apart stable species, which leads to low-density, contaminated samples. Because both of these species are created at low densities, the interaction times for experiments that rely on molecular beams or flow tubes are often too short to have a significant fraction of the molecules react. Acquiring clean samples of radicals in the gas phase and reacting them with ions at low temperatures poses significant difficulties. However, in the last decade, new experimental techniques have become available [9,17–21], which have the promise to overcome some of the experimental challenges.

Recently, these techniques were used to study ion-neutral (nonradical) reactions at low temperatures using laser-cooled ions stored in linear traps. Reactions between laser-cooled atomic ions and neutral species have been demonstrated in several systems [22–28]. Additionally, reactions using sympathetically cooled molecular ions stored in ion traps have been carried out [29–34]. Recent experiments also investigated the influence of the internal state of the ions on the reaction kinetics. In that work, the quantum state of the laser-cooled atomic ion was varied [27,35–40], while in other measurements, the reactivity of the molecular rovibrational state [25,27,41,42] or the conformer was tested [43].

II. Ca^+ + NO REACTIONS

In this work, we present results from reactions between neutral radical molecules and laser-cooled, electrodynamically trapped ions, where the reaction rates are controlled by changing the quantum-state population of the ions. In particular, we study the reactions of laser-cooled $^{40}Ca^+$ at millikelvin temperatures with nitric oxide radicals at room temperature. Since the ions are nearly at rest compared to the neutral molecules, the average collision energy is calculated to be $\bar{E}_{\rm coll}/k_B T \sim 180$ K. There are two possible charged

*lewandoh@colorado.edu

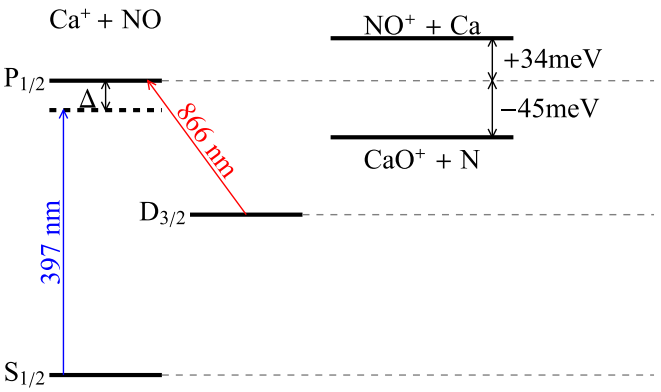

FIG. 1. Comparison of reactant and product energies for the $Ca^+ + NO$ system. The exothermicity of the reaction depends on the quantum state of Ca^+. Excited states of Ca^+ can be populated by excitation on the two cooling laser transitions at 397 and 866 nm. To achieve cooling, the 397-nm laser is red-detuned from resonance by an amount Δ. Only Ca^+ in the $P_{1/2}$ state is energetically allowed to react. The charge exchange product channel barrier is overcome by the thermal energy of neutral NO at 180 K. (Energies not to scale.)

reaction products in this system, CaO^+ and NO^+ [see Eq. (1)], where k_{NO} and k_{CaO} are the rate constants for producing NO^+ and CaO^+, respectively:

$$\begin{aligned} Ca^+ + NO &\xrightarrow{k_{NO}} NO^+ + Ca \\ &\xrightarrow{k_{CaO}} CaO^+ + N. \end{aligned} \tag{1}$$

Subsequent reactions between CaO^+ product ions and NO are energetically forbidden and thus not considered.

The thermochemistry associated with the reactions between Ca^+ and NO was computed with high-level coupled-cluster theory and the HEAT thermochemical protocol [44]. Using these energies, we can determine the exothermic reaction pathways for our system. Laser cooling of Ca^+ simultaneously populates three electronic states: $S_{1/2}$, $D_{3/2}$, and $P_{1/2}$ (Fig. 1). At zero temperature, no reactions can occur when Ca^+ is in either the ground ($S_{1/2}$) or the next lowest-lying excited state ($D_{3/2}$). However, reactions can proceed when Ca^+ is in the $P_{1/2}$ state. Here, the oxygen abstraction process is slightly exothermic [$\Delta E = -45(10)$ meV], while the charge-exchange process is still energetically forbidden by $\Delta E = +34(10)$ meV. For reactions at 180 K, $\bar{E}_{coll} \sim 16$ meV, this channel will also be possible, though only with molecules whose thermal energy exceeds the barrier. Control over both reaction rates is possible by changing the time Ca^+ spends in the $P_{1/2}$ state. In our experiment, this control is accomplished by changing the detuning of the primary cooling laser ($\lambda \sim 397$ nm) from resonance (see Fig. 1).

III. ION-TRAP APPARATUS

The experimental apparatus used to study ion-radical reactions uses a combination of a linear Paul ion trap and a time-of-flight mass spectrometer (TOFMS) [45], similar to Refs. [32], [46], and [47]. The trap allows for accumulation of charged products over the course of a reaction (i.e., several minutes) due to the long lifetime afforded by the large trap depth (2–4 eV). Accumulation of products over such a long time scale makes measurements of ion-radical reactions possible even for reaction rates as slow as one per minute. Additionally, this allows for measurements of accumulated product ions and not just measurements of the depletion of the reactant. This provides the opportunity to map out simultaneous, competing reaction pathways. Once a reaction is complete, the products can be identified by TOFMS. Using measurements of the number of ions at each mass-to-charge ratio, the reaction rates and products of the reaction can be determined. The combination of an ion trap and TOFMS makes studies of very low-density samples of ions and radicals possible.

An experimental run begins by nonresonantly photoionizing (355 nm) a neutral calcium beam and loading the resultant ions into the trap, located in an ultrahigh-vacuum chamber ($<5 \times 10^{-10}$ Torr). $^{40}Ca^+$ ions are then laser-cooled on the $S_{1/2} \rightarrow P_{1/2}$ transition at 397 nm, where the laser is red-detuned by $\Delta = 30$–100 MHz (Fig. 1). Additionally, a repump laser tuned near resonace with the $D_{3/2} \rightarrow P_{1/2}$ transition at 866 nm is used to pump ions that have fallen into the $D_{3/2}$ state back into the cooling cycle. The ions are cooled to a low enough temperature to form a Coulomb crystal [48]. The fluorescence from the Coulomb crystal is imaged onto an intensified CCD camera, so that the initial, absolute number of calcium ions can be determined. Next, NO gas is introduced into the vacuum chamber via a precision leak valve at typical concentrations of 10^7 to 10^8 cm^{-3}. The NO (98.5% purity; Sigma-Aldrich) is passed through an ascarite cell (NaOH:SiO_2 mixture) to remove any residual water and a copper coil filled with a molecular sieve (3-Å pore diameter) submerged in a cold bath at $-115\,^\circ$C to freeze out any N_2O and NO_2. The pressure of NO is measured by a Bayard-Alpert-style ion gauge and Agilent controller (XGS-600). The large ion-trap depth ensures that all charged products will remain trapped and have time to sympathetically cool via interactions with the laser-cooled atomic ions. Once the desired reaction time has elapsed, the trapping potentials are rapidly turned off (<500 ns) and high potentials (~2 kV) are pulsed onto the trap rods to eject ions radially into the TOFMS [45]. The ion current from the microchannel plate detector is converted into a voltage and recorded by a fast oscilloscope (1 GHz). Arrival times and integrated peak areas in the TOFMS spectra are then used to determine the absolute number of ions at each mass-to-charge ratio [45].

IV. REACTION RATE MEASUREMENTS

Reaction rates are determined by repeating experimental runs at different reaction times, while holding the neutral radical concentration and Ca^+ $P_{1/2}$-state population fixed. An example reaction curve is shown in Fig. 2. There, the ion numbers are normalized to the initial number of Ca^+, which is determined from the fluorescence image taken at time $t = 0$. Example images of the crystals after reactions with NO are shown at three times along the reaction curve. The dark bands in the center and along the outer edges of the crystals indicate the presence of nonfluorescing product ions. Solid lines are

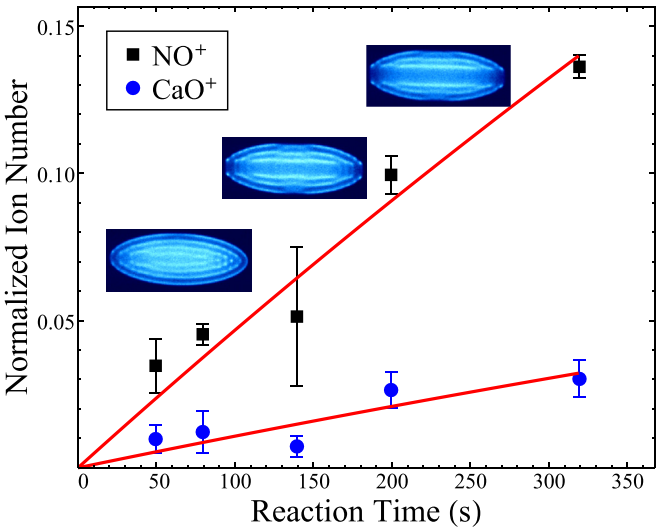

FIG. 2. NO^+ and CaO^+ measured ion numbers as a function of time. Ion numbers are normalized by the initial number of Ca^+ determined from the image captured at $t = 0$. Error bars represent the standard error of the mean of measured ion numbers from five experimental runs at each time point. Solid lines indicate fits to the data using a pseudo-first-order reaction rate model. Also shown are three false-color fluorescence images of the Coulomb crystals taken immediately before ejecting the ions into the TOFMS. Images were taken at $t = 50$, 200, and 320 s. Dark bands in the center and along the outer edges of the crystals indicate the presence of ions that are lighter and heavier than Ca^+, respectively. These ions are the reaction products.

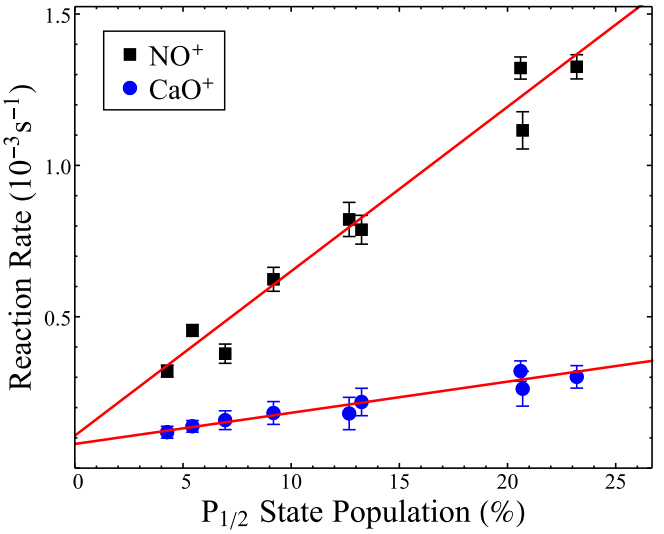

FIG. 3. Measured reaction rates for the two product channels, NO^+ and CaO^+, as a function of the Ca^+ $P_{1/2}$-state population. The NO concentration was $2.3(1) \times 10^8$ cm^{-3} for all of these data. The initial number of Ca^+ ions in the trap was around 600. The slopes of the fit lines are used to determine the 180 K reaction rate constants. The statistical uncertainty in the $P_{1/2}$-state population is smaller than the symbols. There is an offset for the reaction rate at zero excited-state population. However, it corresponds to only a 1%–2% offset in the $P_{1/2}$-state population, which is likely due to a small systematic in determining the absolute state population from the fluorescence.

fits to the data using a pseudo-first-order reaction rate model for each reaction. Explicitly, the model is given by

$$\frac{NO^+(t)}{Ca^+(0)} = \frac{k_{NO}}{k_{NO} + k_{CaO}}\left(1 - e^{-k_{NO}[NO]f_P t}\right), \quad (2)$$

$$\frac{CaO^+(t)}{Ca^+(0)} = \frac{k_{CaO}}{k_{NO} + k_{CaO}}\left(1 - e^{-k_{CaO}[NO]f_P t}\right), \quad (3)$$

where the number of NO^+ and CaO^+ product ions at a given time, t, are normalized by the number of calcium ions at $t = 0$. [NO] is the concentration of neutral NO molecules, and f_P is the fraction of Ca^+ in the $P_{1/2}$ state.

To demonstrate control of the reaction rates by changing the quantum-state populations of the Ca^+, we adjust the 397-nm laser detuning between measurements. The detuning controls the fraction of time an ion spends in the excited $P_{1/2}$ state and, thus, its reactivity. The fraction of time is determined experimentally with the help of the optical Bloch equations [36]. First, we integrate the intensity of the florescence of the entire pure Ca^+ crystal image from the CCD camera as a function of the detuning. Next, we fit these data to the three-level optical Bloch equations. Using this fit, we can calculate the fraction of time the atomic ions spend in the $P_{1/2}$ state based on a single image of the crystal at a known laser detuning. Since the lifetime of the excited state is of the order of a nanosecond, one can model this excitation as a steady-state system, where the fraction of time in the excited state is equal to the fraction of ions that can react.

The results of the quantum-state-controlled reaction can be seen in Fig. 3. There, we keep the NO concentration fixed at $2.3(1) \times 10^8$ cm^{-3} and vary the fraction of ions in the excited $P_{1/2}$ state. We can vary the reaction rate by up to a factor of 5. In our experiment, we were limited in the range of accessible $P_{1/2}$-state populations on the lower end by the decreased cooling rate, which leads to loss of ion crystallization, and on the upper end by the maximum fraction of ions that can be in the $P_{1/2}$ state of the three-level system, assuming the repump laser is on resonance. In total, we are able to vary the population between approximately 5% and 25%.

We were also able to extract the branching ratios and reaction rate constants for the charge exchange channel, k_{NO}, and for the oxygen abstraction channel, k_{CaO}, using the slopes of the linear fits and the fixed NO concentration (see Table I). Note that the NO concentration was estimated from an ion gauge reading with the gas correction factor for NO. To explore a possible systematic effect of the pressure

TABLE I. Results for the two independent determinations of reaction rate constants and branching ratios. The listed uncertainties represent the statistical uncertainty.

	NO concentration	$P_{1/2}$ fraction
k_{NO} (cm^3/s)	$2.3(2) \times 10^{-11}$	$2.7(3) \times 10^{-11}$
k_{CaO} (cm^3/s)	$4.4(7) \times 10^{-12}$	$7(2) \times 10^{-12}$
BR_{NO}	0.8(2)	0.8(1)
BR_{CaO}	0.21(5)	0.16(3)

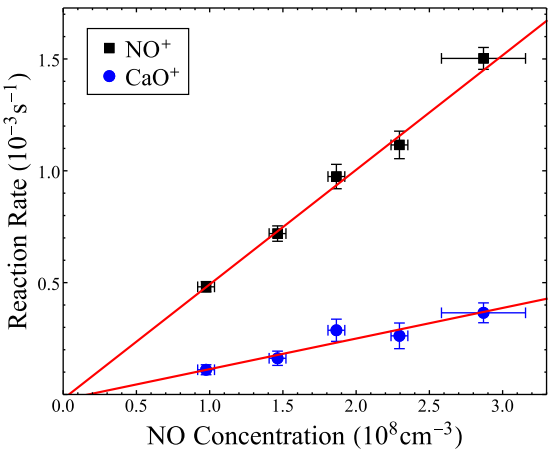

FIG. 4. Measured reaction rates for product channels NO^+ and CaO^+ as a function of the neutral NO concentration in the chamber. The NO pressure in the chamber was varied between 3.4×10^{-9} and 1×10^{-8} Torr to change the NO concentration. For all of these data, the $P_{1/2}$-state population was 19.1% (1.8%). The slopes of the fit lines correspond to the 180 K reaction rate constants.

measurement, we completed an additional experiment to determine the rate constants where any systematic effects likely contribute in different ways.

The second experiment measured the reaction rates for producing NO^+ and CaO^+ at a fixed laser detuning while varying the NO concentration. The results of these measurements can be seen in Fig. 4. Here, we varied the pressure between 3.4×10^{-9} and 1×10^{-8} Torr with a fixed fraction of Ca^+ in the $P_{1/2}$ state of 19.1% (1.8%). The lower end of the range was chosen to be well above the background pressure before the introduction of NO, and the upper end of the range was chosen such that the ions still formed a well-resolved Coulomb crystal. Once again, the rate constants from these measurements were determined by slopes from linear fits to the data and the excited-state population calculated from the fluorescence images (Table I). The rate constants and branching ratios from the two experiments agree to within statistical uncertainties. This agreement gives us confidence in the limited impact of any uncontrolled systematic effects.

V. DISCUSSION

Typical predictions of rate constants using the Langevin capture model do not apply in this situation. This is because one of the channels is endothermic and involves a charge exchange process, neither of which is well characterized by the simple model. Instead, we present a mechanistic model for the reactions. Likely mechanisms for the slightly exothermic chemical reaction and the charge exchange process are shown in Fig. 5. The calcium ions and the NO molecules can combine in four distinct ways, involving A' and A'' electronic states of either singlet or triplet multiplicity. Interaction along the $^3A''$ pathway correlates with the production of a ground-state nitrogen atom and the CaO^+ molecule, while interaction along a $^1A'$ is consistent with the observed charge exchange process. A detailed theoretical characterization of the $^3A''$ and $^1A'$ intermediates is desirable and is the focus of extensive future work. However, the proposed mechanism is plausible and consistent with the observed products.

VI. CONCLUSION

In conclusion, we have demonstrated quantum-state-controlled reactions between laser-cooled Ca^+ ions and neutral NO radicals. We utilized an ion trap to accumulate the charged reaction products over the course of the reaction. By coupling a time-of-flight mass spectrometer to the ion trap, we

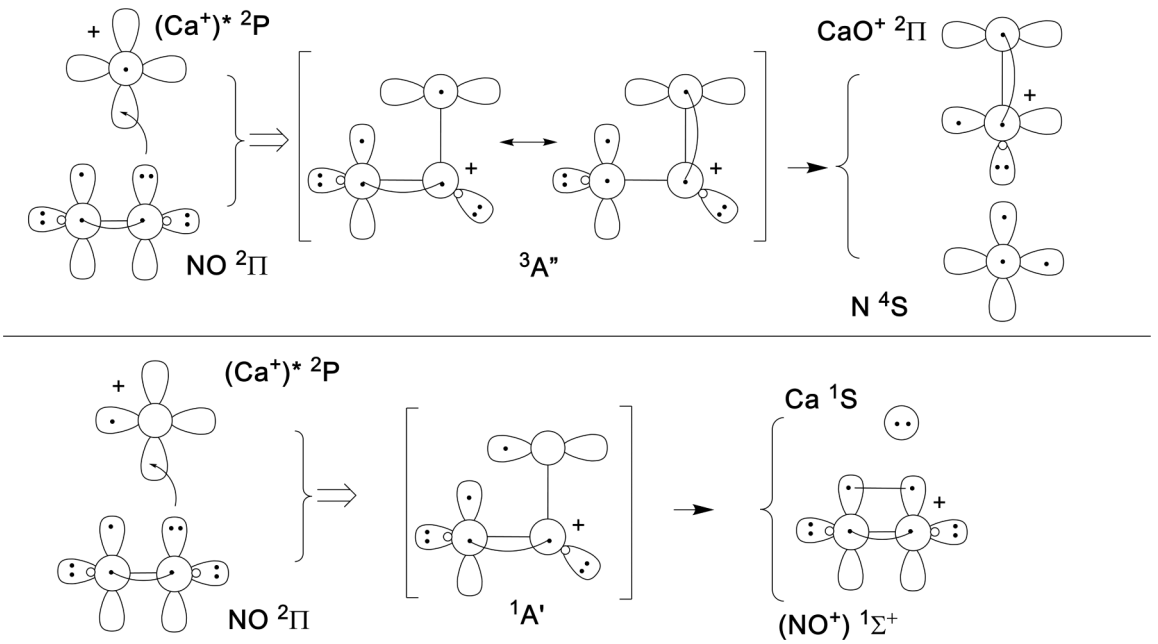

FIG. 5. Top: Generalized valence-bond diagrams that illustrate the processes whereby ^2P calcium atoms react with NO molecules to form CaO^+ and nitrogen atoms in their ground states. Bottom: Charge exchange process that yields Ca atoms and ground-state NO^+.

were able to make simultaneous measurements of the product channels. Using this technique, we made two independent measurements of the reaction rate constants and branching ratios for NO^+ and CaO^+ products at 180 K. A realistic mechanistic model for the two product channels was also presented. In the future, reactants of other important radicals, such as OH and CH, can be introduced to the trapped ions while controlling both the internal rovibrational states and the collision energy through the use of a Stark decelerator. These studies will allow for complete control over the reactants and, thus, lead to a new level of understanding of radical-ion reactions.

ACKNOWLEDGMENTS

This work was supported by the National Science Foundations (Grants No. PHY-1734006 and No. CHE-1464997), Air Force Office of Scientific Research (AFOSR; Grant No. FA9550-16-1-0117), and NIST.

[1] T. P. Snow and V. M. Bierbaum, Annu. Rev. Anal. Chem. **1**, 229 (2008).
[2] V. Wakelam *et al.*, Astrophys. J. Suppl. Ser. **199**, 21 (2012).
[3] K. C. Smyth, S. G. Lias, and P. Ausloos, Combust. Sci. Technol. **28**, 147 (1982).
[4] J. R. Eyler, in *The Chemistry of Combustion Processes. ACS Symposium Series* (American Chemical Society, Washington, DC, 1983), Vol. 249, Chap. 4.
[5] V. Vuitton, R. Yelle, and M. McEwan, Icarus **191**, 722 (2007).
[6] J. H. Westlake, J. H. Waite, N. Carrasco, M. Richard, and T. Cravens, J. Geophys. Res. Space. Phys. **119**, 5951 (2014).
[7] S. I. W. M., Angew. Chem. Int. Ed. **45**, 2842 (2006).
[8] E. Bodo, Phys. Scripta **80**, 048117 (2009).
[9] M. T. Bell and T. P. Softley, Mol. Phys. **107**, 99 (2009).
[10] I. W. M. Smith, Proc. Int. Astron. Union **7**, 361 (2011).
[11] T. Ichino, J. Gauss, and J. F. Stanton, J. Chem. Phys. **130**, 174105 (2009).
[12] D. A. Matthews and J. F. Stanton, J. Chem. Phys. **143**, 204103 (2015).
[13] J. F. Stanton, J. Phys. Chem. Lett. **7**, 2708 (2016).
[14] X. Zhang, V. M. Bierbaum, G. B. Ellison, and S. Kato, J. Chem. Phys. **120**, 3531 (2004).
[15] J. P. Wiens, O. Martinez, S. G. Ard, B. C. Sweeny, A. A. Viggiano, and N. S. Shuman, J. Phys. Chem. A **121**, 8061 (2017).
[16] G. B. I. Scott, D. A. Fairley, D. B. Milligan, C. G. Freeman, and M. J. McEwan, J. Phys. Chem. A **103**, 7470 (1999).
[17] D. Gerlich, Phys. Scr. **1995**, 256 (1995).
[18] M. Schwarz, O. O. Versolato, A. Windberger, F. R. Brunner, T. Ballance, S. N. Eberle, J. Ullrich, P. O. Schmidt, A. K. Hansen, A. D. Gingell, M. Drewsen, and J. R. C. López-Urrutia, Rev. Sci. Instrum. **83**, 083115 (2012).
[19] B. R. Heazlewood and T. P. Softley, Annu. Rev. Phys. Chem. **66**, 475 (2015).
[20] C. Schneider, S. J. Schowalter, K. Chen, S. T. Sullivan, and E. R. Hudson, Phys. Rev. Appl. **2**, 034013 (2014).
[21] S. Willitsch, Adv. Chem. Phys. **162**, 307 (2017).
[22] M. Drewsen, I. Jensen, J. Lindballe, N. Nissen, R. Martinussen, A. Mortensen, P. Staanum, and D. Voigt, Int. J. Mass Spectrom. **229**, 83 (2003).
[23] B. Roth, P. Blythe, H. Daerr, L. Patacchini, and S. Schiller, J. Phys. B **39**, S1241 (2006).
[24] P. F. Staanum, K. Højbjerre, R. Wester, and M. Drewsen, Phys. Rev. Lett. **100**, 243003 (2008).
[25] S. Willitsch, M. T. Bell, A. D. Gingell, S. R. Procter, and T. P. Softley, Phys. Rev. Lett. **100**, 043203 (2008).
[26] F. H. J. Hall, M. Aymar, N. Bouloufa-Maafa, O. Dulieu, and S. Willitsch, Phys. Rev. Lett. **107**, 243202 (2011).
[27] K. Okada, M. Wada, L. Boesten, T. Nakamura, I. Katayama, and S. Ohtani, J. Phys. B **36**, 33 (2003).
[28] W. G. Rellergert, S. T. Sullivan, S. Kotochigova, A. Petrov, K. Chen, S. J. Schowalter, and E. R. Hudson, Phys. Rev. Lett. **107**, 243201 (2011).
[29] T. Baba and I. Waki, J. Chem. Phys. **116**, 1858 (2002).
[30] B. Roth, P. Blythe, H. Wenz, H. Daerr, and S. Schiller, Phys. Rev. A **73**, 042712 (2006).
[31] F. H. J. Hall and S. Willitsch, Phys. Rev. Lett. **109**, 233202 (2012).
[32] K. A. E. Meyer, L. L. Pollum, L. S. Petralia, A. Tauschinsky, C. J. Rennick, T. P. Softley, and B. R. Heazlewood, J. Chem. Phys. A **119**, 12449 (2015).
[33] N. Deb, L. L. Pollum, A. D. Smith, M. Keller, C. J. Rennick, B. R. Heazlewood, and T. P. Softley, Phys. Rev. A **91**, 033408 (2015).
[34] P. Puri, M. Mills, C. Schneider, I. Simbotin, J. A. Montgomery, R. Côté, A. G. Suits, and E. R. Hudson, Science **357**, 1370 (2017).
[35] K. Mølhave and M. Drewsen, Phys. Rev. A **62**, 011401 (2000).
[36] A. D. Gingell, M. T. Bell, J. M. Oldham, T. P. Softley, and J. N. Harvey, J. Chem. Phys. **133**, 194302 (2010).
[37] N. Kimura, K. Okada, T. Takayanagi, M. Wada, S. Ohtani, and H. A. Schuessler, Phys. Rev. A **83**, 033422 (2011).
[38] L. Ratschbacher, C. Zipkes, C. Sias, and M. Köhl, Nat. Phys. **8**, 649 (2012).
[39] A. K. Hansen, M. A. Sørensen, P. F. Staanum, and M. Drewsen, Angew. Chem. Int. Ed. **51**, 7960 (2012).
[40] F. H. Hall, M. Aymar, M. Raoult, O. Dulieu, and S. Willitsch, Mol. Phys. **111**, 1683 (2013).
[41] X. Tong, T. Nagy, J. Y. Reyes, M. Germann, M. Meuwly, and S. Willitsch, Chem. Phys. Lett. **547**, 1 (2012).
[42] A. Kilaj, H. Gao, D. Rösch, U. Rivero, J. Küpper, and S. Willitsch, Nat. Commun. **9**, 2096 (2018).
[43] Y.-P. Chang, K. Długołecki, J. Küpper, D. Rösch, D. Wild, and S. Willitsch, Science **342**, 98 (2013).
[44] A. Tajti, P. G. Szalay, A. G. Csszr, M. Kllay, J. Gauss, E. F. Valeev, B. A. Flowers, J. Vzquez, and J. F. Stanton, J. Chem. Phys. **121**, 11599 (2004).
[45] P. C. Schmid, J. Greenberg, M. I. Miller, K. Loeffler, and H. J. Lewandowski, Rev. Sci. Instrum. **88**, 123107 (2017).
[46] S. J. Schowalter, K. Chen, W. G. Rellergert, S. T. Sullivan, and E. R. Hudson, Rev. Sci. Instrum. **83**, 043103 (2012).
[47] D. Rösch, H. Gao, A. Kilaj, and S. Willitsch, EPJ Tech. Instrum. **3**, 5 (2016).
[48] M. Drewsen, Phys. B Condens. Matter **460**, 105 (2015).